RESEARCH ARTICLE

Cold atmospheric plasma decontamination of SARS-CoV-2 bioaerosols

Alina Bisag[1,2,3] | Pasquale Isabelli[1,4] | Giulia Laghi[1] |
Romolo Laurita[1,3,5] | Giorgio Dirani[6] | Francesca Taddei[6] |
Cristiana Bucci[1,7] | Filippo Capelli[1,3] | Matteo Gherardi[1,3,4] |
Alessandro Paglianti[8] | Vittorio Sambri[6,9] | Vittorio Colombo[1,2,3,4]

[1]Department of Industrial Engineering, Alma Mater Studiorum—University of Bologna, Bologna, Italy

[2]Interdepartmental Center for Industrial Research—Agrifood, Alma Mater Studiorum—University of Bologna, Bologna, Italy

[3]AlmaPlasma s.r.l., Bologna, Italy

[4]Interdepartmental Center for Industrial Research—Advanced Mechanical Engineering Applications and Materials Technology, Alma Mater Studiorum—University of Bologna, Bologna, Italy

[5]Interdepartmental Centre for Industrial Research in Health Sciences and Technologies, University of Bologna, Bologna, Italy

[6]Unit of Microbiology, The Great Romagna Hub Laboratory, Pievesestina (FC), Italy

[7]Department of Medical and Surgical Sciences, Alma Mater Studiorum—University of Bologna, Bologna, Italy

[8]Department of Civil, Chemical, Environmental, and Materials Engineering, Alma Mater Studiorum—University of Bologna, Bologna, Italy

[9]Department of Experimental, Diagnostic, and Specialty Medicine, Alma Mater Studiorum—University of Bologna, Bologna, Italy

Correspondence
Romolo Laurita, Interdepartmental Center for Industrial Research—Advanced Mechanical Engineering Applications and Materials Technology, Alma Mater Studiorum—University of Bologna, via Terracini 24, 40131 Bologna, Italy.
Email: romolo.laurita@unibo.it

Funding information
Regione Emilia-Romagna, Grant/Award Number: 2014–2020 European Regional Development Fund Emilia-Romagna Regional Operational Program

Abstract
Bioaerosols (aerosolized particles with biological origin) are strongly suspected to play a significant role in the transmission of Severe Acute Respiratory Syndrome Coronavirus 2 (SARS-CoV-2), especially in closed indoor environments. Thus, control technologies capable of effectively inactivating bioaerosols are urgently needed. In this regard, cold atmospheric pressure plasma (CAP) can represent a suitable option, thanks to its ability to produce reactive species, which can exert antimicrobial action. In this study, results; on the total inactivation of SARS-CoV-2 contained in bioaerosols treated using CAP generated in air are reported, demonstrating the possible use of CAP systems for the control of SARS-CoV-2 diffusion through bioaerosols.
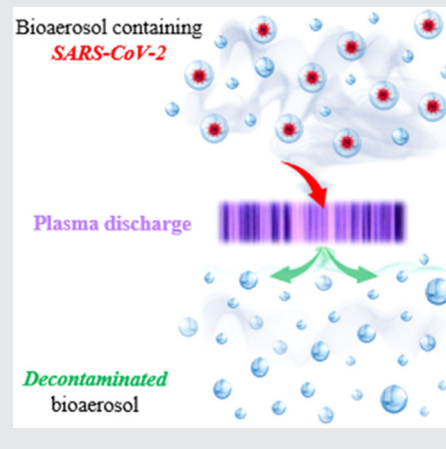
1 | INTRODUCTION

Nowadays, bioaerosols (defined as aerosolized particles with biological origin) have become an important topic in our daily life because they are strongly suspected to play a significant role in the transmission of Severe Acute Respiratory Syndrome Coronavirus 2 (SARS-CoV-2), especially in poorly ventilated indoor environments. SARS-CoV-2 (identified in Wuhan, China, in December 2019[1,2]) can be released by infected persons in small droplets (within a respirable size range) while breathing, talking, sneezing, coughing, or laughing, with a viral load that generally depends on the location within the respiratory tract from which the droplets originated.[3,4] As reported by Smith et al.,[5] speech produces a single-peak drop size distribution (1–10 μm), whereas cough produces a double-peak distribution (1–10 and 100–1000 μm). The trajectory of large particles (60–100 μm) depends strongly on the air velocity and the relative humidity; moreover, these could travel at a speed of 50 m/s and can reach a horizontal distance of 6 m. While coughing, the particle's speed is about 10 m/s, leading to horizontal dispersion of about 3 m, whereas, during exhalation, the particles have a trajectory of about 1 m. On the contrary, the smaller particles emitted (diameter < 5 μm), also called aerosols, could contain viral agents and could remain potentially infectious over time and distances longer than 6 m.[3,6–9] In terms of this, Smith et al.[5] found that SARS-CoV-2 aerosols can remain viable in indoor air for more than 3 h.[10]

As the spread of SARS-CoV-2 in indoor environments has become a crucial issue (with strong social, health, and economic impacts), control technologies capable of effectively inactivating bioaerosols are urgently needed. Different technologies are commonly used for air cleaning, such as air filters or UV lamps. Nevertheless, these methods often provide unsatisfactory results. For example, filters do not inactivate pathogens but merely trap them. Pathogens captured on filters can remain infectious for extended periods and then they can be released back into the air. For this reason, filters require frequent maintenance and must be replaced frequently (approximately every 12–18 months).[11,12] In addition, in HVAC (heating, ventilation, and air conditioning) systems, filters cause pressure losses that can be significant and impact the cost of a ventilator. UV-C technology is well established for the inactivation of pathogens, particularly on surfaces. However, UV-C radiation is limited by the line-of-sight requirement and by the shadow effect as it cannot penetrate opaque surfaces. In the air, the potential to inactivate pathogens is reduced considering the low residence times of particles.[11,12] Furthermore, prolonged or incorrect UV exposure can cause numerous health hazards. It is known that UV-C rays can induce mutations in skin cells that can result in cancer; thus, UV-C exposure should be limited in humans as much as possible.[11,12] For these reasons, it is interesting to investigate new technologies to reduce airborne transmission of COVID-19, such as cold atmospheric plasma (CAP) devices. Indeed, CAP, an ionized gas able to produce a blend of bioactive components (e.g., reactive oxygen and nitrogen species [RONS], electric field, UV ray), can inactivate the aerosolized virus through various oxidative processes, damaging nucleic acid, and proteins and lipids, causing aggregation of viruses.[13,14]

Moreover, CAP can also act as a particle filter, thanks to the effect of the associated electric field in imparting charge-driven filtration due to the induction of negative charging of particles.[15] For this reason, several studies have focused on the use of CAP for the decontamination of air from potential pathogens, for example, viruses.[16,17] In contrast to other technologies, CAP can inactivate the airborne virus with an efficiency comparable to that of filters requiring less or no maintenance. Furthermore, systems based on plasma technology, installed in HVAC, potentially cause a lower pressure drop compared to filters requiring fewer energy costs.

In terms of this aspect, the authors demonstrated that CAP can be used successfully for the degradation of SARS-CoV-2 RNA in bioaerosols[18] and food packaging surfaces.[19]

In this study, the virucidal activity of CAP treatment evaluated by means of direct genome amplification and Vero E6 cell culture is reported. These results are supported by data on the electrical and gas-phase chemical characterization of the CAP system and on the droplet distribution of the bioaerosol.

2 | MATERIAL AND METHODS

2.1 | Plasma source and electrical and gas phase characterization

CAP was generated using a parallel-plate dielectric barrier discharge (DBD) configuration, as described previously.[18] Figure 1a shows the CAP device used for bioaerosol inactivation, composed of two aluminum

electrodes ($5 \times 150 \times 2$ mm) encased within two PMMA (polymethyl methacrylate) supports and fixed by epoxy resin. Both the electrodes were covered by 2-mm-thick ceramic layers ($\varepsilon_r = 6$–8), and, thanks to the presence of two T-section PMMA walls, a gap of 2 mm was maintained between them (Figure 1b).

As shown in Figure 2, the plasma device was driven by a micropulsed high-voltage generator (AlmaPULSE; Alma-Plasma s.r.l.), applying a peak-to-peak voltage (V) of 56 kV$_{p-p}$ and a frequency (f) of 4 kHz. A single-jet Blaustein Atomizer (BLAM; CH Technologies), fed with an air flow of 1.2 slpm by a digital mass flow controller (EL-FLOW; Bronkhorst), was used to aerosolize a SARS-CoV-2 suspension, produced as reported in Section 2.1, in a syringe fixed on a syringe pump (Legato®100; kdScientific); the bioaerosol was flown through the interelectrode gap and exposed to the plasma discharge.

The applied voltage (V) and the current (I) were measured using a high-voltage probe (Tektronix P6015A) positioned on the high-voltage cable and a current probe (Pearson 6585) positioned on the ground cable. The corresponding waveforms were recorded using a digital oscilloscope (Tektronix DPO4034, 350 MHz, 2.5 GSa/s). The average discharge power (P) dissipated over the applied voltage period (T) was determined using the following formula:

$$P = \frac{1}{T} \int_0^T V(t)I(t)dt. \tag{1}$$

Optical absorption spectroscopy (OAS) was used to evaluate the concentration of ozone, one of the long-lived species produced by CAP, in the downstream, to have information about the chemistry induced by CAP treatment, focusing on long-lived species.

The setup for OAS is the same reported in Simoncelli et al.[20]; a deep UV LED, characterized by a narrow band spectrum radiation, was used as a light source. With the aim of investigating the plasma afterglow, the UV light beam was focused inside a measurement cell connected to the plasma source by a 20-cm-long tube (4 mm internal diameter). The measurement cell had two quartz optical windows and enabled measurements without any interference from the plasma discharge emission in the optical analysis. The light beam passed through the measurement cell and was collected into a 500-mm spectrometer (Acton SP2500i; Princeton Instruments) to spectrally resolve the light beam in the UV, VIS, and near-infrared regions. The width of the inlet slit of the spectrometer was fixed at 25 μm for OAS acquisitions, and a grating with a resolution of 150 mm^{-1} was used. A photomultiplier tube (PMT-Princeton Instruments PD439) connected to a fast oscilloscope (Tektronix DPO40034) was used as the detector, allowing fast acquisitions with a time resolution of 40 ms. The PMT amplification factor was maintained constant for all acquisitions. To ensure identical initial conditions, fresh air was flushed for 30 s inside the plasma source before every measurement.

To quantitatively evaluate the species concentrations from absorption measurements, the Lambert–Beer law has to be taken into account:
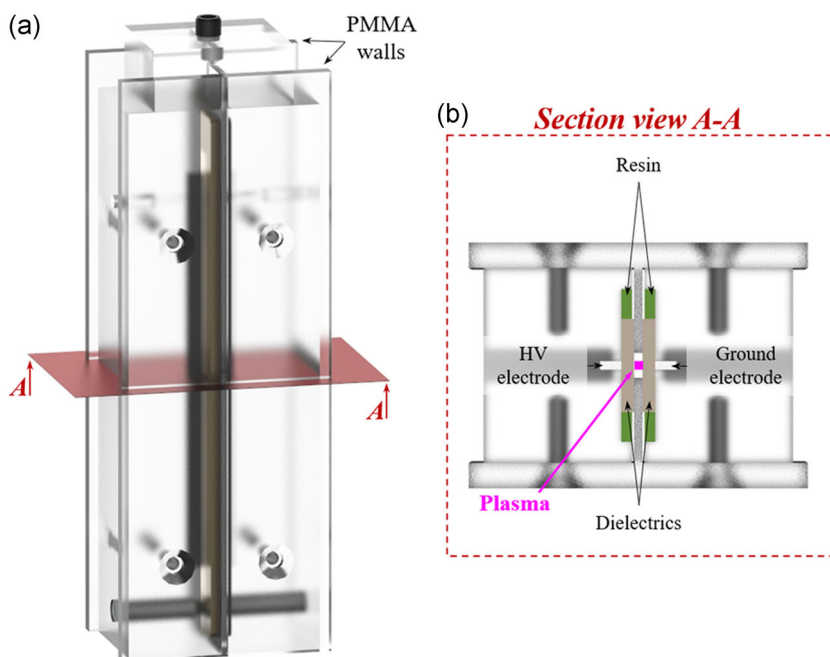
$$\frac{I}{I_0} = e^{(-L\sigma n)}, \tag{2}$$

FIGURE 1 (a) Direct DBD plasma source used for the inactivation of airborne pathogens. (b) Section view, highlighting the high-voltage (HV) and ground electrodes covered by dielectric material. DBD, dielectric barrier discharge; PMMA, polymethyl methacrylate
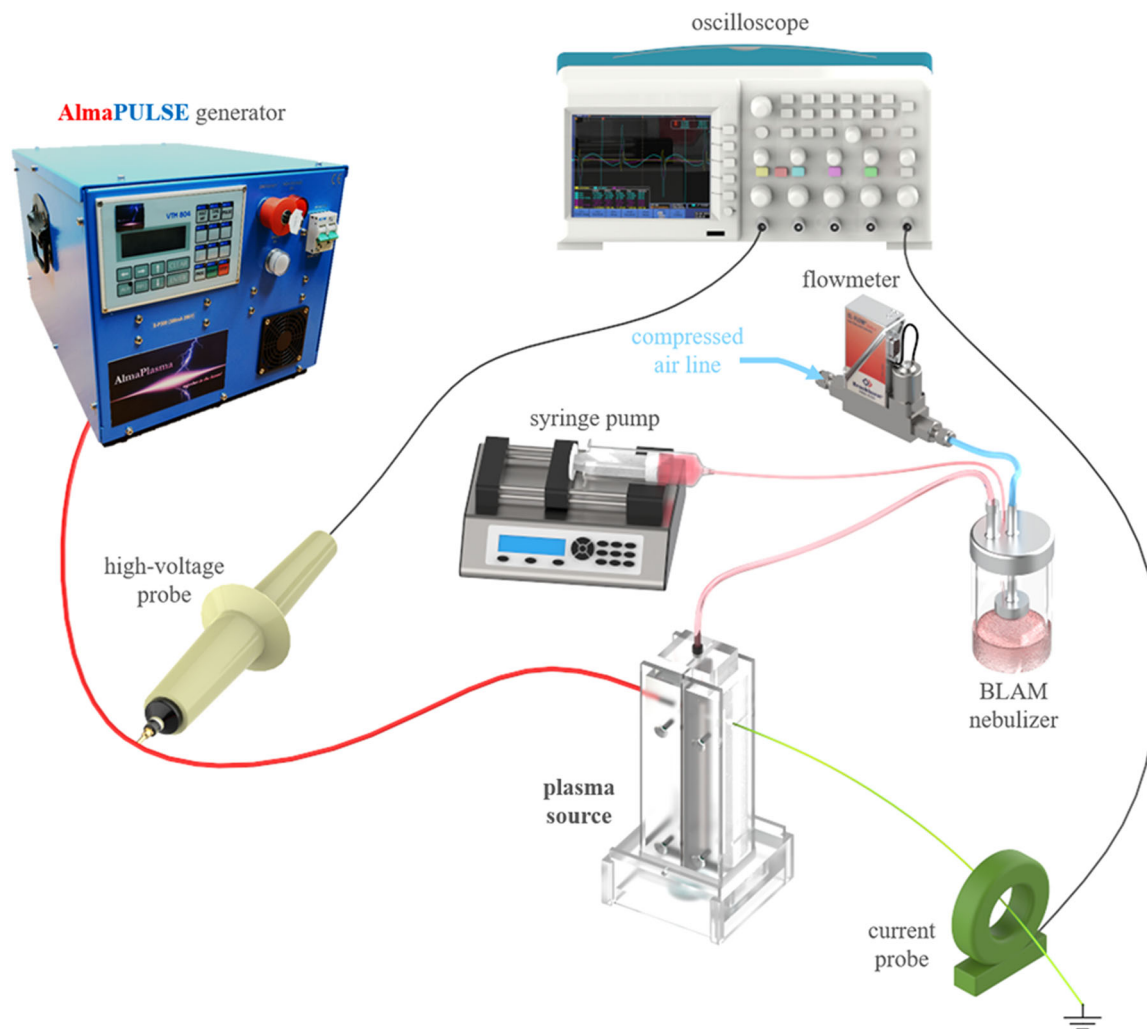
FIGURE 2 Setup for the electrical characterization

where I/I_0 is the ratio between the initial light intensity I_0 and the light intensity I after an optical path length L and n is the concentration of absorbers. The absorption cross-section σ is a function of the wavelength ($\sigma = \sigma(\lambda)$).

In general, when N species absorb at the same λ_j wavelength, the Lambert–Beer equation can be re-written as follows:

$$\frac{I}{I_0}\bigg|_j = e^{\left(-L\sum_{i=1}^{N}\sigma_{i,j}n_i\right)},$$ (3)

where $\sigma_{i,j}$ is the absorption cross-section of the i-species at λ_j and the ratio between the light intensities I and I_0 is referred to as the j-wavelength. The concentration n of each absorbing species can thus be obtained from the following expression, where the suffix k indicates a generic absorber:

$$n_k = -\frac{1}{L\sigma_{k,j}}\ln\left(\frac{I}{I_0}\bigg|_j\right) - \sum_{i\neq k}^{N}\frac{\sigma_{i,j}}{\sigma_{k,j}}n_i,$$ (4)

A wavelength value of 253 nm was selected to perform the study; the corresponding absorption cross-section for O_3 is $(1.12 \pm 0.02)E{-}17$. This wavelength was defined, in accordance with Moiseev et al.,[21] to maximize the absorption of the molecules relevant to our study while minimizing the contribution, and thus, the disturbance of other absorbing molecules.

For all experiments, the optical path length L is 8 cm and the contributions of background radiation and spontaneous plasma emission were duly taken into account in the data processing, subtracting them from the acquired values of I and I_0. All measurements were performed three times.

2.2 | Particle distribution evaluation

Additionally, the real-time measurement of the particle distribution at the outlet of the single-jet BLAM was carried out using a laser diffraction system SPRAYTECH (Malvern; Panalytical), as detailed by Bisag et al.[18] To perform this type of measurement, the outlet of the single-jet BLAM was positioned between the transmitter and the receiver modules; these were fixed on the optical bench and spaced at about 100 mm. The acquisition was performed for about 120 s, and the resulting data were analyzed using SPRAYTECH software.

2.3 | Preparation of viral stocks

One clinical isolate of SARS-CoV-2 obtained from an RT-PCR-positive nasopharyngeal swab of a patient suffering from COVID-19 in March 2020 was originally cultured in a Vero E6 cell line monolayer as described by La Scola et al.[22] and, before starting the culture to increase the viral titer, an aliquot of the original cell supernatant was tested by multiplex reverse-transcription polymerase chain reaction (RT-PCR) (FilmArray Respiratory Panel; bioMerieux) to exclude the possibility of coinfection by other respiratory tract viruses.

The VERO E6 cells were propagated using the protocol of Ammerman et al.[23] The day before infection, approximately 1×10^6 cells were seeded in a T25 flask using 5% fetal bovine serum (FBS) Dulbecco's modified Eagle medium (DMEM) and then incubated overnight at 37°C in a humidified, 5% CO_2 atmosphere-enriched chamber. Before the infection process, the culture medium was aspirated and discarded, and the cells were gently washed with phosphate-buffered saline. Five milliliters of fresh 2% FBS DMEM were added to each T25 flask. The cells were confluent up to 80%, but less than 100% to avoid contact inhibition to which the cells are subjected.[24,25] 0.5 ml of the clinical sample was added to a 25-cm^2 VERO E6 cell flask, and the cell culture supernatant was harvested after 72 h of incubation and titrated according to Ramakrishnan,[26] with minor modifications. After 72 h, the supernatant was added to a 25-cm^2 flask under the same conditions. This process was repeated four times to increase the viral concentration. Three aliquots of the supernatant were thus tested with RT-PCR to determine the titer.

The titration was performed using a PCR method. The supernatant obtained from the flask was processed using a Nextractor (Genolution Inc.) for RNA extraction and amplified using a CFX96 real-time PCR real time termocycler (CFX96; Bio-Rad) using See-Gene Allplex SARS-CoV-2 RT-PCR (AllPlex SARS-CoV-2; SeeGene). This method was targeted at four different SARS-CoV-2 genes (namely, N, E, S, and RdRp), and the positive results were defined according to the dedicated software interpretation (SeeGene Viewer software). Using this assay, a mean of the three Ct values was obtained and entered into the conversion file,[24] which yields the number of copies of RNA/μl through the Ct. In particular, the correlation was obtained using the following equation $y = -0.3062x + 10.50$, SE (slope) = 0.01427, SE (Y-intercept) = 0.3596, $r^2 = 0.9127$, $p < 0.0001$.[24] (Table 1).

2.4 | Evaluation of CAP efficacy in inactivating SARS-CoV-2

The stock corresponding to a virus concentration of approximately 1×10^9 RNA copies/μl was diluted 1:1000 to prepare the required volume of the working viral suspension at approximately 1×10^6 RNA copies/μl. The required volume of the working viral suspension was prepared in a minimum essential medium (EuroClone) without FBS (EuroClone).

To evaluate the CAP activity on bioaerosol containing SARS-CoV-2, the syringe was loaded with 20 ml of the above-mentioned viral suspension and fixed in the syringe pump to deliver a liquid flow rate of 0.852 ml/min necessary to produce the bioaerosol inside the nebulizer. It was flowed through the plasma region for 150 s and collected in a 35-mm well (containing 1 ml of distilled water) at a distance of 5 mm from the plasma source orifice. Untreated samples (Untreated) were collected using the same procedure; however, the plasma discharge was not generated and was thus not exposed to CAP treatment. In addition, the RT-PCR and cell culture assay were also performed on an identical aliquot of viral suspension directly from the working viral suspension, as a control (CNT).

Two different methods were used to establish the efficacy of the CAP treatments to inactivate SARS-CoV-2: a direct genome amplification using a commercial RT-PCR technique (AllPlex SARS-CoV-2; SeeGene) and Vero E6 cell culture.

2.4.1 | Multiplex PCR

The direct genome identification was performed using the above-reported method standard of RT-PCR according to the manufacturer's instructions: the CAP-treated

TABLE 1 PCR (polymerase chain reaction) titration of the viral stock with cycle threshold (Ct) and respective RNA copies/µl

Titration	Ct value (N gene) of the stock supernatant	Average RNA copies/µl (N gene)	Average Ct value (N gene) of the stock supernatant	Average RNA copies/µl (N gene)
Virus stock (First replicate)	4.84	1042 298 229	4.91	992 236 405 = ~10^9
Virus stock (Second replicate)	4.93	978 214 283		
Virus stock (Third replicate)	4.95	964 517 251		

viral suspension was extracted from the collection vial and amplified. The Ct (cycle threshold) values reported in the results are those identified for the N gene amplification; also, it is the gene used in digital PCR.[24]

2.4.2 | Plasma-treated viruses with vero cells

0.5 ml of viral suspension collected at the end of the CAP treatment was inoculated into a 25-cm² Vero E6 cell confluent monolayer under the same conditions as those used for preparing the viral stock. After 24, 48, and 72 h of incubation at 37°C in a 5% CO_2 atmosphere, 0.5 ml aliquot of the cell culture supernatant was collected and processed by RT-PCR as described above. Each experiment was performed in duplicate. The Ct values in Table 2 are for the N gene amplification. From these values, it was possible to perform the titration by correlating with the line obtained in digital PCR.[24]

3 | RESULTS

3.1 | Electrical characterization of the DBD plasma source and ozone concentration

Figure 3 shows the current and applied voltage waveforms for the DBD plasma source operating at 56 kV_{p-p}, with a fixed frequency of 4 kHz. During the applied voltage period (250 µs), two active discharge phases can be easily distinguished by the presence of multiple spikes on the current waveform (at around 22 and 144 µs), which correspond to filamentary discharges (with a duration of about 10 ns) typical of DBDs operated in air at atmospheric pressure.[27] A proper evaluation of the average discharge power is essential since this parameter directly affects the production of RONS responsible for antimicrobial action.[28] The average discharge power calculated directly from the measured current and voltage using formula (1) is 4.86 ± 0.12 W.

3.2 | Ozone concentration

The ozone concentration was determined in the measurement cell 20 cm downstream. The ozone concentration reached a steady-state regime at 870 ± 40 ppm, 20 s after the plasma ignition, as reported in Table 2. This concentration is representative of the ozone production in the plasma discharge and represents only part of the plasma bioactive components (i.e., UV rays, RONS, electric field) able to inactivate viruses and bacteria.

FIGURE 3   Current and applied voltage
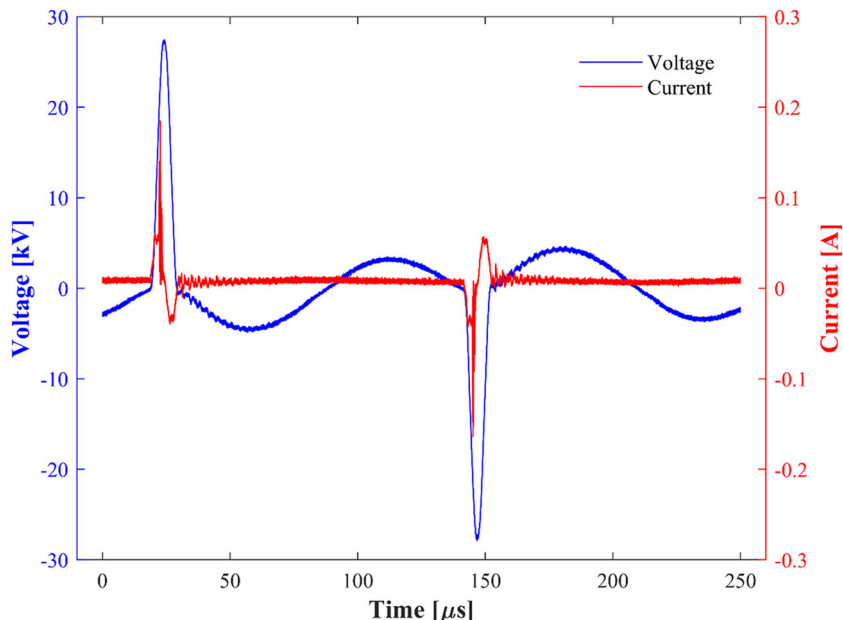waveforms at 56 kV_{p-p} and 4 kHz

TABLE 2   Ozone concentration

Distance from the orifice (cm)	Plasma on time (s)	O_3 concentration (ppm)
20	20	870 ± 40

3.3 | Characterization of the distribution of the droplets in the bioaerosol

The evaluation of the Sauter (d_{32}, surface area moment mean) and the De Broukere (d_{43}, volume or mass moment mean) diameters was performed by real-time laser diffraction analysis. The two quantities were evaluated as:

$$d_{32} = \frac{\sum_{i=1}^{N} x_i d_i^3}{\sum_{i=1}^{N} x_i d_i^2}, \qquad (2)$$

$$d_{43} = \frac{\sum_{i=1}^{N} x_i d_i^4}{\sum_{i=1}^{N} x_i d_i^3}, \qquad (3)$$

where x_i is the numerical fraction of the total particle number associated with a diameter d_i and N is the number of discrete size classes used, equal to $d_{32} = 3.58\,\mu m$ and $d_{43} = 5.57\,\mu m$.

The Sauter diameter represents the diameter of a droplet with the same volume/surface area ratio as the entire sample. Therefore, it provides information on processes in which the active surface area is important. The De Broukere diameter is the diameter obtained by weighting the droplet size distribution by the volume of the droplets. Compared to the Sauter diameter, it is more sensitive to the larger particles; they contain most of the volume of the sample.

By setting the optimal distance between the atomizing nozzle and the liquid surface contained inside the glass jar, the Sauter diameter of particles generated using the BLAM nebulizer is in the same range of those particles emitted as aerosols (i.e., $d < 5\,\mu m$) that could potentially be infectious in closed environments, as previously reported.[3,6–9]

Figure 4a shows the frequency of each class as a function of the droplet sizes. It is noteworthy that the most frequent class (about 15.2%) is that of the droplets with a diameter of $1.47\,\mu m$. Figure 4b shows how the volume of the liquid phase is distributed between each class of droplets. Obviously, the peak moves toward droplets of larger diameter with respect to the condition shown in Figure 4a. Figure 4b shows that 8.7% of the liquid phase is due to the droplets with a diameter of $4.31\,\mu m$. Because it is possible to assume that the volumetric concentration of the pathogen does not depend on the droplet size, the distribution of the volumetric fraction can be assumed to be the distribution of the pathogen in the emitted aerosol.

3.4 | CAP treatment of aerosolized SARS-CoV-2

3.4.1 | Direct genome identification

Before the CAP treatment, an RT-PCR assay was performed using the viral suspension that was fluxed
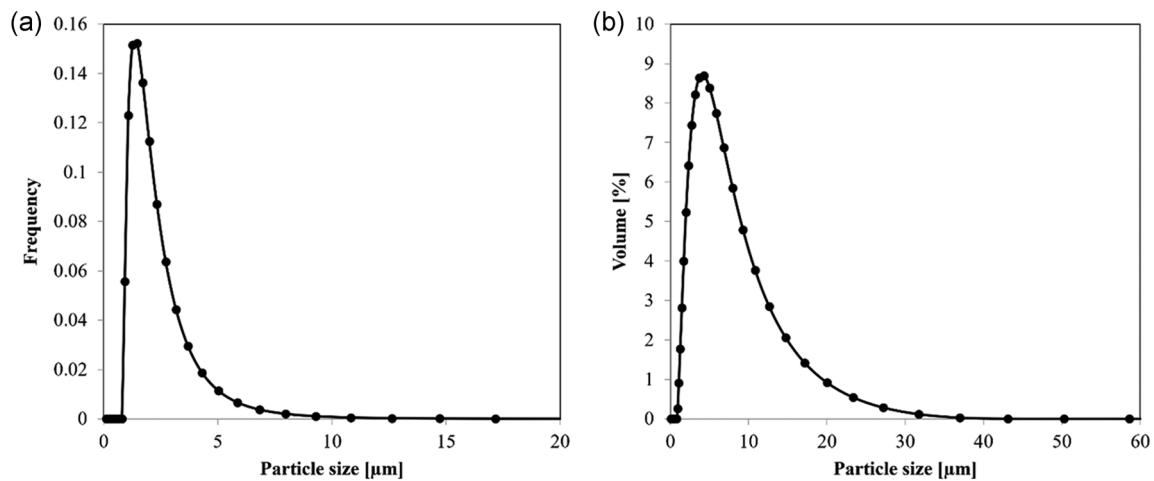
FIGURE 4 Size distribution of aerosol droplets at the outlet of the single-jet Blaustein Atomizer: (a) distribution of the number fraction and (b) distribution of the volumetric fraction

through the inactive CAP device. The mean Ct value for the N gene was 25: this is likely due to a dilution effect generated by the flux inside the CAP device. After the treatment with CAP, the results of the RT-PCR test were completely negative.

3.4.2 | Vero E6 cell culture

In Table 3, data obtained in RT-PCR with the related RNA copies/μl 24, 48, and 72 h after the incubation are reported. As reported in Table 3, no positive results were found when the RT-PCR was performed on cell cultures inoculated with the virus suspension treated with CAP. Pictures of the flasks of Vero E6 cell culture are shown below in Figure 5. It can be clearly observed that in the flasks inoculated with the virus CNT, there was a decrease in the Ct value corresponding to an increase in virions demonstrable with the growth of RNA copies/μl, causing a visible cytopathic effect that ends at 72 h with the destruction of the monolayer. On the contrary, in the flasks in which the CAP-treated virus stock was inoculated, the RT-PCR was not able to detect any amplification, and actually in the cells, no cytopathic effects were observed.

4 | DISCUSSION

The possibility that SARS-CoV-2 virions contained in aerial materials emitted by infected patients could contribute to the contamination of the environment has been raised since the very beginning of the current pandemic as it was a major concern during the first

SARS outbreak in 2003.[29] As a consequence, two fields of investigation are needed: the first method should be dedicated to determining the time that is necessary for SARS-CoV-2 virions to maintain their infectivity when located on different surfaces.[19] The second approach should be the investigation of different chemical and physical methods to reduce the infectivity of SARS-CoV-2 isolated virions in the environment. Both the above-listed strategies will play a pivotal role in the effective control of the COVID-19 pandemic.

One of the major issues in defining the optimal strategy for reducing the infectivity of environmentally dispersed SARS-CoV-2 virions is the balance between the effective reduction of the infectivity in respect to the potential damage that chemical or physical treatment could cause to the structure of the materials. CAP is a possible treatment to reduce the presence of infecting SARS-CoV-2 virions in the air and surface of environmental materials. CAP has been proven to be safe and effective in damaging capsid and nucleic acids thanks to the content of RONS generated during treatment[13] and inactivating SARS-CoV-2 on surfaces.[30]

In this study, the effect of CAP on aerosolized SARS-CoV-2 viral particles is shown asefficient in inactivating the virus, even ifa low power (less than 9 W) was used to generate CAP. No residual viral RNA was detectable by RT-PCR after CAP treatment of the SARS-CoV-2 aerosolized particles within a short treatment time, thus suggesting high efficacy of the CAP. This result indicates that the structural integrity of the target sequences of genes used for the RT-PCR was destroyed. As the viral RNA is contained in a complex protein structure, whose integrity is required

TABLE 3 Average Ct of the N gene in CNT, untreated, and CAP treated samples

Treatment condition	Average Ct value (N gene) after 24 h of culture	Average RNA copies/µl (N gene) after 24 h of culture	Average Ct value (N gene) after 48 h of culture	Average RNA copies/µl (N gene) after 48 h of culture	Average Ct value (N gene) after 72 h of culture	Average RNA copies/µl (N gene) after 72 h of culture
CNT	26	345	24	1416	13	3 306 739
CAP-treated	ND	ND	ND	ND	ND	ND
Untreated	30	20	27	170	16	398 841

Abbreviations: CAP, cold atmospheric plasma; Ct, cycle threshold; CNT, control; ND, not determined (negative).
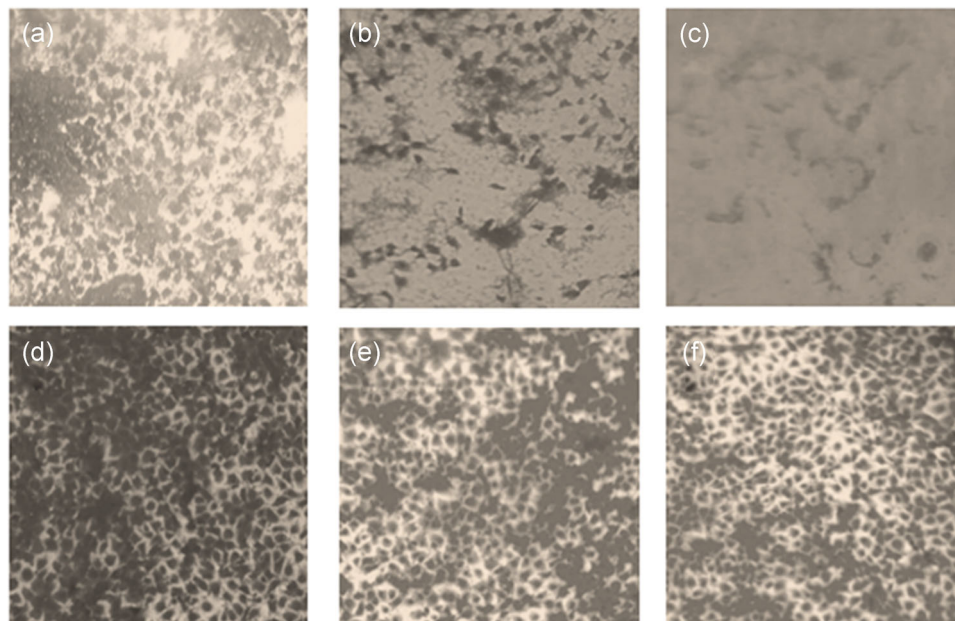
FIGURE 5 The upper panel shows Vero E6 cell cultures for the untreated viral suspension at 24 h postinfection (a), 48 h postinfection (b), and 72 h postinfection (c). The pictures at the bottom show the Vero E6 cell culture for the cold atmospheric plasma (CAP)-treated suspension at 24 h postinfection (d), 48 h postinfection (e), and 72 h postinfection (f). No cytopathic effect is visible on the CAP-treated suspension. X100 magnification

for the infection of eukaryotic cells, it is highly likely that the CAP treatment damaged the structural architecture of the SARS-CoV-2 virions. To prove this hypothesis, the efficacy of CAP treatment was confirmed by inoculating an aliquot of the CAP-treated viral suspension in a very permissive cell line. The complete absence of viral replication after 3 days of incubation provides definitive evidence that the infectivity of SARS-CoV-2 was completely abolished with the CAP treatment. The results obtained in this study open a wide perspective on the possibility to apply CAP system for the reduction of the infectivity of SARS-CoV-2 particles in closed environment. It is worth noting that several bioactive components of the CAP induce the inactivation of the viruses; among them, the ozone concentration in a measurement cell is reported. Indeed, on the one hand, ozone can contribute to the inactivation of the virus; on the other hand, it has to be monitored due to its toxicity at high concentrations.[31]

To develop a plasma-based system for decontamination of bioaerosols useful in real-life environments, it is important to conduct more in-depth investigations of the chemistry induced by CAP in the gas phase and evaluate the mechanisms behind the plasma virucidal effect. Moreover, it will be important to identify the most suitable system for ozone abatement (e.g. carbon filters) to reach a concentration of ozone in a closed room below the short-term exposure limit of 0.06 ppm, according to Occupational Safety and Health Administration (https://www.osha.gov/chemicaldata/9).

5 | CONCLUSION

To our knowledge, this study is the first to demonstrate the total inactivation of SARS-CoV-2 contained in bioaerosol by means of CAP. The presented results provide the basis for the development of a novel device based on CAP technology able to inactivate bioaerosols in a closed environment and thus reduce the spread of COVID-19.

DATA AVAILABILITY STATEMENT
Data available on request from authors.

ORCID

Alina Bisag https://orcid.org/0000-0003-0982-9002
Pasquale Isabelli https://orcid.org/0000-0003-0600-2755
Giulia Laghi https://orcid.org/0000-0003-1815-4342
Romolo Laurita http://orcid.org/0000-0003-1744-3329
Giorgio Dirani https://orcid.org/0000-0001-7554-9653
Francesca Taddei https://orcid.org/0000-0003-2707-2082
Filippo Capelli https://orcid.org/0000-0002-8243-0594
Matteo Gherardi http://orcid.org/0000-0001-6995-6754
Alessandro Paglianti https://orcid.org/0000-0003-3295-9227
Vittorio Sambri https://orcid.org/0000-0002-5012-7355
Vittorio Colombo https://orcid.org/0000-0001-9145-198X

REFERENCES

[1] H. Li, F. Y. Leong, G. Xu, Z. Ge, C. W. Kang, K. H. Lim, *Phys. Fluids* **2020**, *32*, 113301.

[2] M. Abkarian, H. A. Stone, *Phys. Rev. Fluids* **2020**, *5*, 102301.

[3] L. Morawska, D. K. Milton, *Clin. Infect. Dis.* **2020**, *2019*, 2311.

[4] G. Buonanno, L. Stabile, L. Morawska, *Environ. Int.* **2020**, *141*, 105794.

[5] S. H. Smith, G. A. Somsen, C. van Rijn, S. Kooij, L. van der Hoek, R. A. Bem, D. Bonn, *Phys. Fluids* **2020**, *32*, 107108.

[6] G. R. Johnson, L. Morawska, Z. D. Ristovski, M. Hargreaves, K. Mengersen, C. Y. H. Chao, M. P. Wan, Y. Li, X. Xie, D. Katoshevski, S. Corbett, *J. Aerosol Sci.* **2011**, *42*, 839.

[7] J. Yan, M. Grantham, J. Pantelic, P. J. B. de Mesquita, B. Albert, F. Liu, S. Ehrman, D. K. Milton, *Proc. Natl. Acad. Sci. U. S. A.* **2018**, *115*, 1081.

[8] W. G. Lindsley, J. D. Noti, F. M. Blachere, R. E. Thewlis, S. B. Martin, S. Othumpangat, B. Noorbakhsh, W. T. Goldsmith, A. Vishnu, J. E. Palmer, K. E. Clark, D. H. Beezhold, *J. Occup. Environ. Hyg.* **2015**, *12*, 107.

[9] V. Stadnytskyi, C. E. Bax, A. Bax, P. Anfinrud, *Proc. Natl. Acad. Sci. U. S. A.* **2020**, *117*, 11875.

[10] N. van Doremalen, T. Bushmaker, D. H. Morris, M. G. Holbrook, A. Gamble, B. N. Williamson, A. Tamin, J. L. Harcourt, N. J. Thornburg, S. I. Gerber, J. O. Lloyd-Smith, E. de Wit, V. J. Munster, *N. Engl. J. Med.* **2020**, *382*, 1564.

[11] H. Mohamed, G. Nayak, N. Rendine, B. Wigdahl, F. C. Krebs, P. J. Bruggeman, V. Miller, *Front. Phys.* **2021**, *9*, 286.

[12] G. Berry, A. Parsons, M. Morgan, J. Rickert, H. Cho, *Environ. Res.* **2022**, *203*, 111765.

[13] E. H. Choi, H. S. Uhm, N. K. Kaushik, *AAPPS Bull.* **2021**, *31*(5), 1.

[14] A. Filipić, I. Gutierrez-Aguirre, G. Primc, M. Mozetič, D. Dobnik, *Trends Biotechnol.* **2020**, *38*, 1278.

[15] G. Nayak, A. J. Andrews, I. Marabella, H. A. Aboubakr, S. M. Goyal, B. A. Olson, M. Torremorell, P. J. Bruggeman, *Plasma Processes Polym.* **2020**, *17*, 1900269.

[16] J. Romero-Mangado, D. Nordlund, F. Soberon, G. Deane, K. Maughan, S. Sainio, G. Singh, S. Daniels, I. T. Saunders, D. Loftus, M. Meyyappan, J. Koehne, R. P. Gandhiraman, *Biointerphases* **2016**, *11*, 011009.

[17] A. C. K. Lai, A. C. T. Cheung, M. M. L. Wong, W. S. Li, *Build. Environ.* **2016**, *98*, 39.

[18] A. Bisag, P. Isabelli, R. Laurita, C. Bucci, F. Capelli, G. Dirani, M. Gherardi, G. Laghi, A. Paglianti, V. Sambri, V. Colombo, *Plasma Processes Polym.* **2020**, *17*(10), 1.

[19] F. Capelli, S. Tappi, T. Gritti, A. C. de Aguiar Saldanha Pinheiro, R. Laurita, U. Tylewicz, F. Spataro, G. Braschi, R. Lanciotti, F. Gomez Galindo, V. Siracusa, S. Romani, M. Gherardi, V. Colombo, V. Sambri, P. Rocculi, *Appl. Sci.* **2021**, *11*, 4177.

[20] E. Simoncelli, J. Schulpen, F. Barletta, R. Laurita, V. Colombo, A. Nikiforov, M. Gherardi, *Plasma Sources Sci. Technol.* **2019**, *28*, 095015.

[21] T. Moiseev, N. Misra, S. Patil, P. Cullen, P. Bourke, K. Keener, J. Mosnier, *Plasma Sources Sci. Technol.* **2014**, *23*, 065033.

[22] B. La Scola, M. Le Bideau, J. Andreani, V. T. Hoang, C. Grimaldier, P. Colson, P. Gautret, D. Raoult, *Eur. J. Clin. Microbiol. Infect. Dis.* **2020**, *39*, 1059.

[23] N. Ammerman, M. Beier-Sexton, A. Azad, *Curr. Protoc. Microbiol.* **2008**, *Appendix 4*, 11(1), 1.

[24] M. Brandolini, F. Taddei, M. M. Marino, L. Grumiro, A. Scalcione, M. E. Turba, F. Gentilini, M. Fantini, S. Zannoli, G. Dirani, V. Sambri, *Viruses* **2021**, *13*(6), 1.

[25] F. Hasler, A. Duda, T. M. Kündig, P. Johansen, *STAR Protoc.* **2021**, *2*, 100824.

[26] M. A. Ramakrishnan, *World J. Virol.* **2016**, *5*, 85.

[27] X. Zhang, M. S. Cha, *J. Phys. D. Appl. Phys.* **2013**, *46*, 415205.

[28] U. Kogelschatz, B. Eliasson, M. Hirth, *Ozone: Sci. Eng.* **1988**, *10*, 367.

[29] J. C. Luongo, K. P. Fennelly, J. A. Keen, Z. J. Zhai, B. W. Jones, S. L. Miller, *Indoor Air* **2016**, *26*, 666.

[30] Z. Chen, G. Garcia Jr., V. Arumugaswami, R. E. Wirz, *Phys. Fluids* **2020**, *32*, 111702.

[31] B. Bayarri, A. Cruz-Alcalde, N. López-Vinent, M. M. Micó, C. Sans, *J. Hazard. Mater.* **2021**, *415*, 125658.